RSC Advances

PAPER

View Article Online
View Journal | View Issue

Cite this: *RSC Adv.*, 2016, **6**, 64285

Substituent effect on the spin state of the graphene nanoflakes

Reyes Flores, Ana E. Torres and Serguei Fomine*

The effect of the substituents on the electronic properties of graphene nanoflakes possessing a high spin ground state, has been studied at D3bj dispersion corrected B3LYP/cc-pVDZ, and CAS/6-31G(d) levels of theory. The results of DFT and CAS calculations qualitatively agree with each other. The substituents affect the nature of the ground state. The electron withdrawing substituents, especially these with cyano groups favor the singlet ground state. The effect of the electron donating groups is more erratic. They can promote both high and low spin ground states. The side groups affect the topology of singly occupied molecular orbitals, modifying exchange interactions. Hence, depending on the type of substituents, one or another spin state could be favored. The calculations confirmed that the origin of the high spin ground state in these systems is attributed to the nondisjointed character of the occupied orbitals causing strong exchange coupling between the electrons. The substitution of the nanoflake increases the band gap and their reorganization energies.

Received 1st June 2016
Accepted 27th June 2016

DOI: 10.1039/c6ra14279f

www.rsc.org/advances

Introduction

Since some decades ago, the π-conjugated systems have gained researchers attention as an alternative for organic semiconductor applications.[1,2] The organic semiconductors could be arranged in two big groups, the first encompasses conjugated polymers and the second one small molecules. Although in recent years another group has emerged,[3] consisting of large two-dimensional π-conjugated systems.[4]

Recent theoretical studies have suggested that the medium sized and large graphene derivatives have a multiconfigurational and sometimes a polyradicalic ground state.[4–6] Another face of the coin of two dimensional π-conjugated systems is the high spin organic molecules. The π-electron of a conjugated hydrocarbon can be considered as an assembly of spins. The determinant of lowest energy, associated to the largest coefficient in the ground state wavefunction, is the one in which each atom bearing an α spin is surrounded by adjacent β spins, and reciprocally. The most-alternant spin distribution does not necessarily correspond to $M_s = 0$ (even number of sites), or $M_s = 1/2$ (odd number of sites), and may exhibit more α than β spins. According to the Ovchinnikov rule, the ground-state total spin in alternant systems is given by the difference between the number of sites of different "colors" ($S = 1/2(N_\alpha - N_\beta)$).[7,8] As far as planar alternant conjugated hydrocarbons are concerned, up until now there have not yet been found any counterexample to this rule. However, it has recently been discovered[9] that a series of graphene nanoflake like structures (Fig. 1) first described by Perepichka *et al.*[10] have high spin ground state. The total spin of the ground state rises with size from 2 (4 unpaired electrons) for **2D-PA-36** to 6 (12 unpaired electrons) for **2D-PA-144**. This example is a clear violation of the Ovchinnikov rule since all mentioned systems are fully conjugated planar alternant hydrocarbons with $N_\alpha = N_\beta$. This violation can be related with rapid closing of HOMO–LUMO gap with size for singlet states in these systems. Therefore, the small members of **2D-PA** series[9] possess singlet ground state as predicted by the Ovchinnikov rule. They have large HOMO–LUMO gap which closes rapidly with size reaching 0.26 eV for **2D-PA-36** and further dropping to 0.10 eV for **2D-PA-64**.

The total spin of the ground state in these systems is determined by the exchange interactions.[11] Electron-exchange interactions in organic molecules are controlled by the Pauli exclusion principle, which leads to either ferromagnetic or antiferromagnetic coupling pattern. The molecules with large HOMO–LUMO gap normally show strong antiferromagnetic coupling. A different situation arises for molecules where the molecular orbitals (MO's) are approximately equal in energy leading to singly occupied MO's (SOMO's). According to Borden and Davidson, the two SOMO's can be classified as either disjoint (not spatially coinciding) or nondisjoint (spatially coinciding).[12] Disjoint orbitals are the orbitals have very different coefficients on common atoms, while in the case of nondisjoint orbitals the coefficients on common atoms are close in value.

Instituto de Investigaciones en Materiales, Universidad Nacional Autónoma de México, Apartado Postal 70-360, CU, Coyoacan, Mexico DF 04510, Mexico. E-mail: fomine@unam.mx

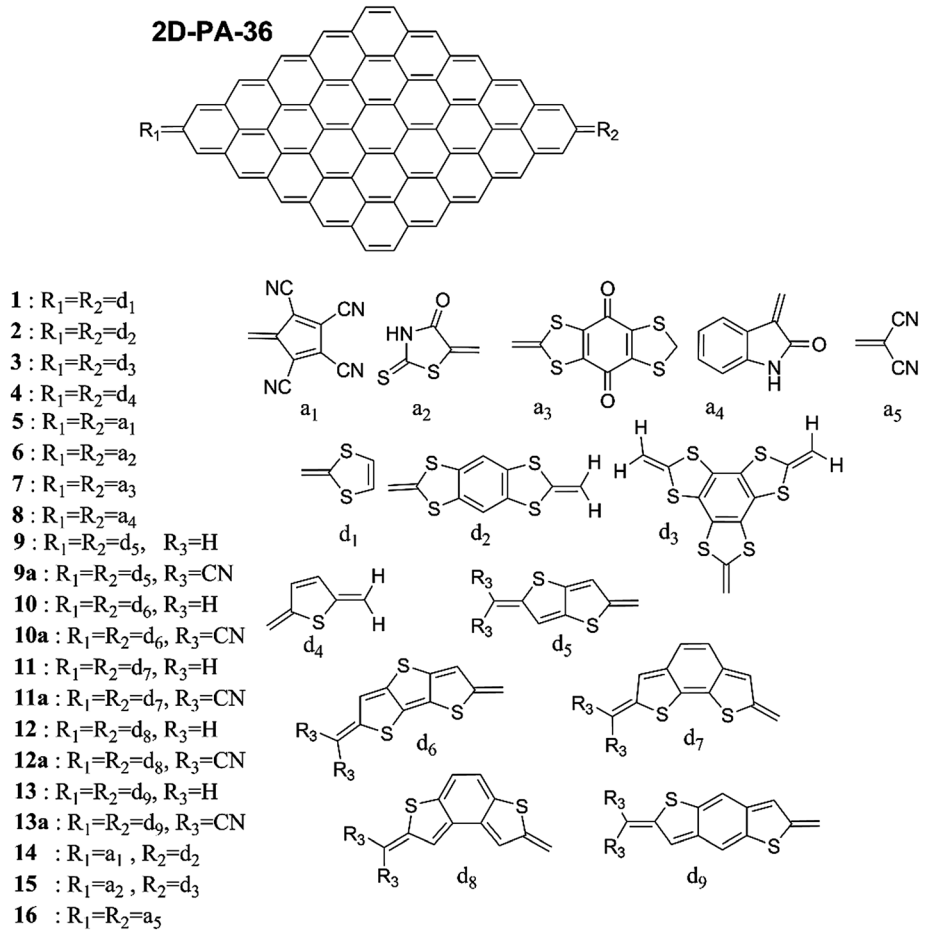

Fig. 1 Structures of substituted nanoflake derivatives.

For disjoint SOMOs, exchange coupling is very weak, leading to a singlet ground state. For nondisjoint SOMOs, exchange coupling is strong and ferromagnetic leading to the high spin ground state.[12–14]

It is interesting to explore the effect of substituents on the nature of the high spin ground state of the **2D-PA** molecules since substituents modify the molecular orbitals, thus changing the nature of the ground state. The electron-withdrawing and donating groups seem to be the most promising for this purpose. When attached to π-conjugated chains they modify the HOMO–LUMO (HLG) gap and promote intramolecular charge transfer.[15,16]

Selected substituents are shown in (Fig. 1). They all can be divided into two large groups; the electron donating and the electron withdrawing substituents. The first group include substituents d_1–d_9. They have low ionization potentials (IP)'s thanks to sulfur(II) atoms. The second group includes substituents from a_1 to a_5. They have electronegative sp or sp^2 atoms inferring high electron affinities (EA)'s to these groups. We have selected the smallest representative of **2D-PA** series (**2D-PA-36**) which still possess high spin (quintet) ground state. The molecular structures that have been studied have two donor and/or electron-withdrawing substituents linked to the core structure (Fig. 1).

Computational details

All geometry optimizations were carried out at B3LYP/cc-pVDZ theory level,[17] and D3bj dispersion corrected.[18] When triplet instability of the ground state has been detected, the structures were reoptimized using unrestricted broken symmetry DFT (BS-UB3LYP). Both neutral and ionic species have been optimized for different multiplicities in order to locate the lowest energy spin state.

Single point calculations at complete active space (CAS) level were run for these systems where the high spin ground state was detected at DFT level. Since the importance of the static correlations decreases with the multiplicity, the largest difference between the single and multireference methods prevails for the low spin states. The CAS calculations were carried out using 6-31G(d) basis set for all atoms, the active space consisted of 10 electrons and 10 orbitals. This was the largest possible active space. CAS calculations were performed using Gaussian 09 rev. D.01 code.[19]

The energy gaps (E_g) were estimated as the lowest excitation energy calculated with the time dependent implementation of M062X functional (TD-M06-2X/cc-pVDZ//B3LYP-D3(BJ)/cc-pVDZ).[20] This method reproduces well the lowest excitation energy of organic dyes.[21,22]

M06-2X functional contains (54%) of exact exchange, thus improving the performance of this functional for the low overlap excitations. Moreover, TD-M06-2X/cc-pVDZ//B3LYP-D3(BJ)/cc-pVDZ model reproduces well the lowest excitation energy of recently synthesized aza analogue of nanocene: octaazanonacene-8,19-dione (1.95 eV *vs.* 1.82 eV (exp)).[23] For the unstable closed shell solution, the broken symmetry unrestricted singlet solution was used as the reference state.

The hole reorganization energies (λ_+) of GNRs were estimated as following:

$$\lambda_+ = (E_n^+ - E_n) + (E_+^n - E_+)$$

where E_n and E_+ are the energies of the neutral and cationic species in their lowest energy geometries, while E_n^+ and E_+^n are the energies of the neutral and cationic species with the geometries of the cationic and neutral species, respectively. The electron reorganization energy (λ_-) is defined similarly:

$$\lambda_- = (E_n^- - E_n) + (E_-^n - E_-)$$

In this case, E_n and E_- are the energies of the neutral and the anionic species in their lowest energy geometries, while E_n^- and E_-^n are the energies of the neutral and anionic species with the geometries of the anionic and neutral species, respectively.

Results and discussion

As it has been demonstrated earlier[9] the pristine nanoflake (**2D-PA-36**) ($R_1 = R_2 = CH_2$) has a quintet ground state with four unpaired electrons. According to the Ovchinnikov rule **2D-PA-36** must have a singlet ground state, since it is alternant, plane and totally conjugated hydrocarbon with equal number of atoms with different "color". On the other hand, the Ovchinnikov rule cannot be strictly applied to the substituted nanoflakes, since some of them are not plane, all of them have heteroatoms and some of them are not alternant. Therefore, the only system which clearly demonstrates the violation of the Ovchinnikov rule is the pristine nanoflake.

The relative energy for closed and open shell singlet, triplet, quintet and septet states are shown in the Table 1. According to the DFT calculations all structures presented triplet instability. This means that in all cases closed shell singlet solutions are unstable. Eight structures (**2**, **5**, **7**, **8**, **11**, **12**, **13**, **15**, **16**) showed singlet polyradicalic ground state (PRS) which corresponds to the BS-UDFT solution, while **9**, **9a**, **10**, **10a**, **13a** and **14**, had a triplet ground state, the rest of the systems have quintet ground state with four unpaired electrons (**1**, **3**, **4**, **6** and **12a**). As seen, none of the substituents promotes higher multiplicities than quintet of the original **2D-PA-36** system. However, some of the substituents reduce the multiplicity of the ground state to triplet or even singlet.

Evidently, the substituents have a strong impact on the nature of the ground state of the studied nanoflake systems. For instance, the electron withdrawing side groups, in particular these with cyano substituents, favor the singlet ground state.

Table 1 Relative electronic energies[a] of studied systems (kcal mol^{-1}) at B3LYP-D3bj/cc-pVDZ level for closed shell singlet (S0), triplet (T), quintet (Q), septet states (S) and singlet polyradicalic state (PRS)

Structure	S0	PRS	T	Q	S
2D-PA-36	26.53	23.22	3.31	0.00	9.18
1	—[b]	10.68	1.40	0.00	7.33
2	36.01	0.00	5.77	4.23	11.53
3	30.79	7.24	1.55	0.00	7.29
4	30.81	1.87	2.91	0.00	7.49
5	0.40	0.00	5.50	9.48	—[b]
6	20.05	7.66	15.16	0.00	7.29
7	22.05	0.00	4.61	3.27	10.56
8	26.01	0.00	3.51	4.14	—[b]
9	31.58	2.19	0.00	1.88	9.43
9a	26.51	5.96	0.00	2.13	9.68
10	30.39	5.44	0.00	2.60	10.21
10a	25.86	5.38	0.00	2.73	10.21
11	32.02	0.00	3.23	2.47	10.13
11a	25.59	0.80	0.00	3.25	10.89
12	34.63	0.00	4.44	4.01	11.64
12a	20.53	0.80	0.39	0.00	7.66
13	32.33	0.00	3.03	2.10	9.74
13a	25.65	4.95	0.00	3.13	10.76
14	11.89	4.94	0.00	5.18	—[b]
15	26.53	0.00	5.79	4.25	11.56
16	21.31	0.00	4.88	4.25	11.56

[a] Using the ground state energy as the reference state. [b] SCF not converged.

Thus, all three systems having cyano groups as a part of the side group possess singlet ground state with a notable singlet-triplet gap (around 5 kcal mol^{-1}, Table 1). The effect of the electron

Table 2 $\langle S^2 \rangle$ expectation values for the singlet polyradicalic broken symmetry state (PRS), triplet (T), quintet (Q) and septet (Sep) states at B3LYP-D3bj/cc-pVDZ level

Structure	PRS	T	Q	Sep
2D-PA-36	3.04	3.59	6.15	12.21
1	2.19	3.58	6.13	12.20
2	2.66	3.58	6.13	12.20
3	2.48	3.58	6.13	12.20
4	2.55	3.16	6.19	12.27
5	0.48	2.13	6.17	[a]
6	2.08	3.85	6.14	12.21
7	2.62	3.15	6.20	12.27
8	2.68	3.61	6.16	[a]
9	2.61	3.66	6.21	12.28
9a	2.12	3.64	6.18	12.26
10	2.15	3.67	6.22	12.29
10a	2.13	3.65	6.19	12.26
11	2.60	3.17	6.20	12.27
11a	2.62	3.65	6.18	12.25
12	2.66	3.18	6.20	12.27
12a	2.14	3.15	6.18	12.25
13	2.63	3.18	6.21	12.28
13a	2.14	3.65	6.19	12.26
14	1.12	2.33	6.19	[a]
15	2.67	3.58	6.13	12.20
16	2.68	3.32	6.15	12.22

[a] SCF not converged.

donating groups on the nature of the ground state is not as straightforward as that of the electron withdrawing groups. The electron donating groups, d_1, d_3, d_4 and d_8 promote high spin quintet states, while other donor substituents promote lower triplet or ever singlet polyradicalic states. The most interesting case is **6** where the gap between the ground quintet state and the second stable state (singlet) achieved 7.66 kcal mol^{-1} which is larger than in pristine **2D-PA-36**, (3.31 kcal mol^{-1}, triplet) at DFT level. The opposite case is the molecule **5** with singlet polyradicalic ground state and the singlet–triplet gap of 5.50 kcal mol^{-1} (Table 1). Moreover, the restricted and unrestricted singlet solutions in the nanoflake **5** are almost degenerated implying the mostly single reference character of the ground state. This is also reflected in relatively small $\langle S^2 \rangle$ expectation values for the singlet broken symmetry unrestricted solution of only 0.48 (Table 2).

The CAS single point calculations of **5** produce multi-configurational wavefunction with the squared expansion

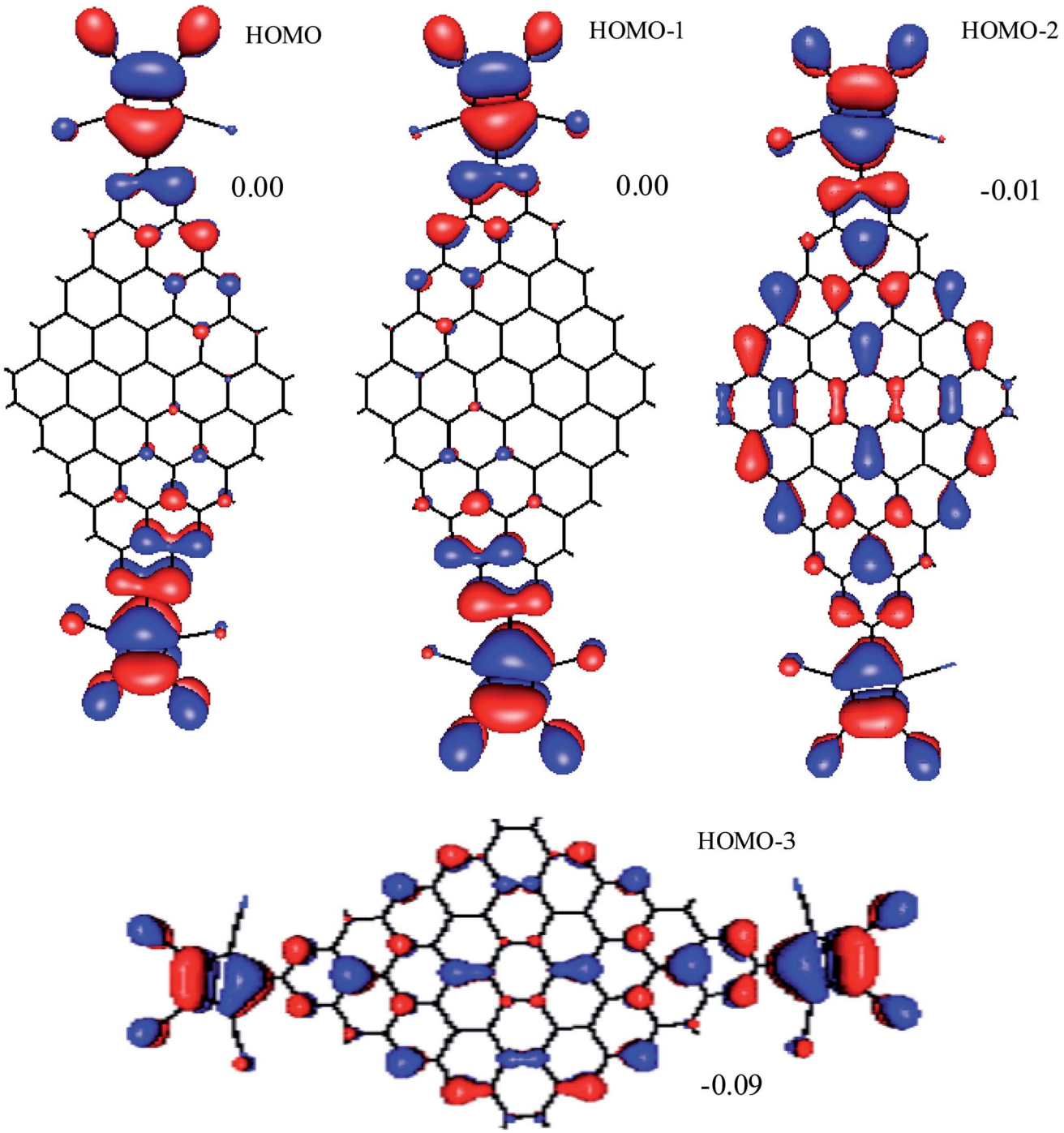

Fig. 2 Highest SOMO's of the nanoflakes **5** and their relative energies in eV.

coefficient of the dominant closed shell singlet configuration of 0.90 indicating the single reference singlet ground state.

Fig. 2 and 3 show the first occupied molecular orbitals (HOMO, HOMO−1, HOMO−2 and HOMO−3) for these two cases which are actually SOMO's and also **2D-PA-36** SOMO's for the comparison purpose. As seen both system **6** and **2D-PA-36** with the quintet ground state have highly nondisjoint orbitals resulting in the strong exchange coupling and, therefore, in the ferromagnetic ordering. On the other hand, strong electron withdrawing substituents of the system **5** modify SOMO's topology distributing the electron density over the electron withdrawing groups. HOMO, HOMO−1, HOMO−2 and HOMO−3 in **5** become more disjoint, thus reducing the exchange coupling between the electrons, favoring polyradicalic low spin state. Therefore, the substituents change topology of SOMO's thus modifying the exchange interaction. Depending on the substituents type, one or another spin state can be favored.

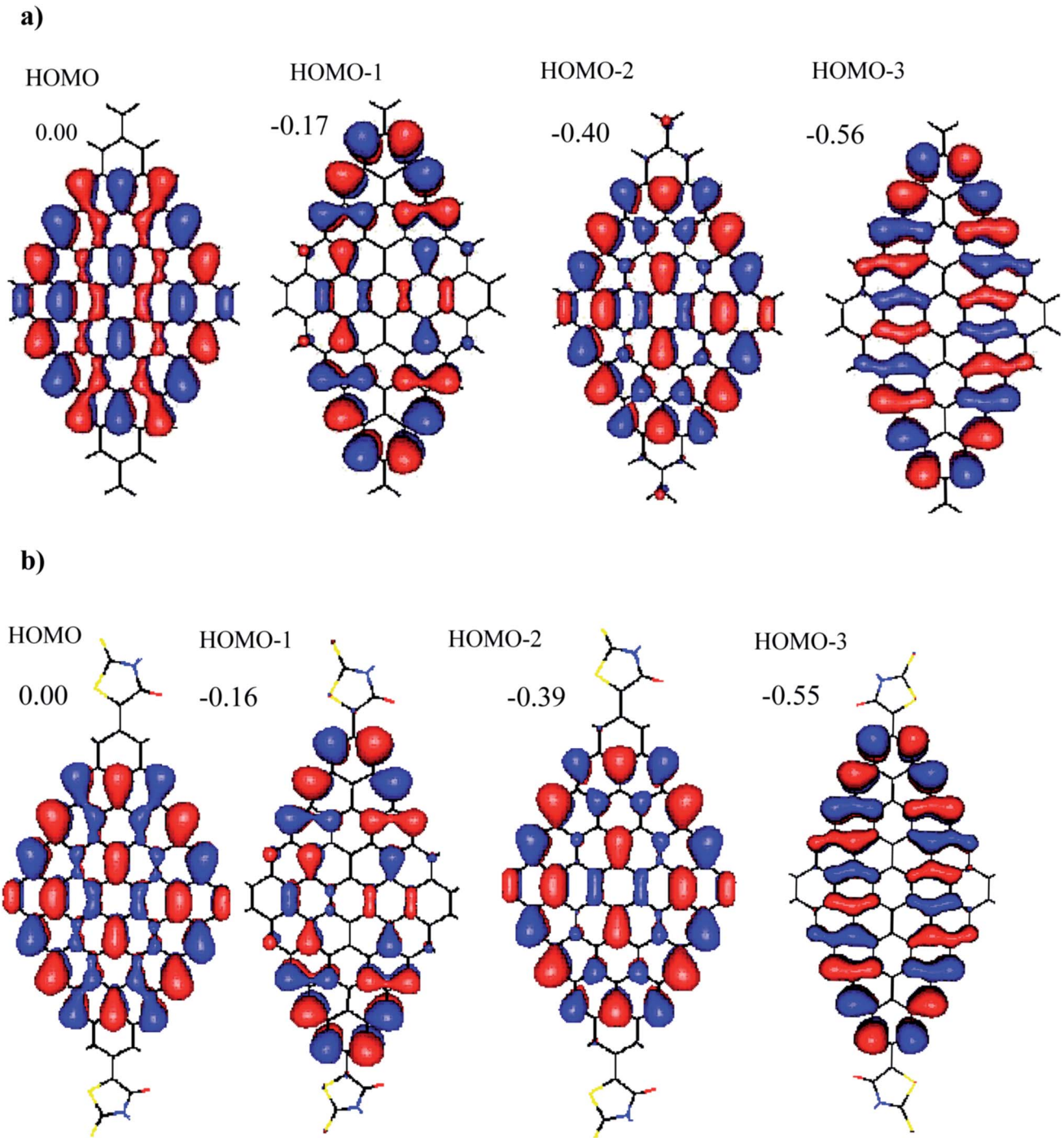

Fig. 3 Highest SOMO's of pristine nanoflake **2D-PA-36** (a) and **6** (b) and their relative energies in eV.

Table 3 Relative electronic energies (kcal mol^{-1}) at CAS/6-31G(d) theory level for singlet (S), triplet (T) and quintet (Q) states at B3LYP-D3bj/cc-pVDZ optimized geometry of the respective multiplicity

Structure	S[a]	T	Q
2D-PA-36	21.2	2.4	0.00
1	0.00	7.00	9.28
3	9.66	15.89	0.00
4	2.78	1.59	0.00
6	4.04	12.09	0.00
12a	0.93	14.98	0.00

[a] BS-UB3LYP-D3bj/cc-pVDZ optimized geometry.

Table 4 Squared CI expansion coefficients of CAS/6-31G(d) wavefunction for singlet (S), triplet (T) and quintet (Q) geometries obtained at B3LYP-D3bj/cc-pVDZ optimized geometries

	S[a]	T	Q
Structure	2222200000	2222aa0000	222aaaa000
2D-PA-36	0.180	0.770	—
1	0.191	0.258	0.904
3	0.205	0.282	0.910
4	0.215	0.329	0.909
6	0.239	0.542	0.930
12a	0.238	0.853	0.867

[a] BS-UB3LYP-D3bj/cc-pVDZ optimized geometry.

$\langle S^2 \rangle$ expectation values for the different systems and the different multiplicities are shown in the Table 2. The theoretical values for the triplet, quintet and septet are of **2**, **6** and **12**, respectively. As seen, these values are greatly differ from the theoretical ones for BS-UDFT solution and also for triplets indicating notable spin contamination for all the nanoflakes except for **5**, as it has been mentioned above. For the nanoflakes **5** the $\langle S^2 \rangle$ expectation values are of 0.48 and 2.13 for BS-DFT singlet and triplet solutions respectively. For the higher multiplicities, however, quintet and septet, $\langle S^2 \rangle$ expectation values are close to the theoretical values indicating almost no spin contamination due to decreasing importance of static correlation for the high spin states.

Table 5 Ionization potential (IP) and electron affinity (EA) obtained at B3LYP/cc-pVDZ level of theory (eV)

Structure	IP	EA
2D-PA-36	5.10	2.25
1	4.92	2.17
2	5.06	2.08
3	5.00	2.31
4	5.08	2.33
5	6.72	4.49
6	5.31	3.05
7	5.35	3.04
8	5.25	2.36
9	5.18	2.33
9a	5.56	3.27
10	5.21	2.35
10a	5.55	3.27
11	5.22	2.34
11a	5.52	3.35
12	5.32	2.29
12a	5.34	3.52
13	5.21	2.37
13a	5.54	3.39
14	5.69	3.72
15	5.28	2.51
16	5.88	3.13

Table 6 Relative energies (kcal mol^{-1}) of cationic and anionic species for doublet (D) quartet (Qrt) and sextet (Sxt) spin states, as well as their $\langle S^2 \rangle$ expectation values (in baskets) obtained at B3LYP-D3bj/cc-pVDZ level theory

	Cations			Anions		
Structure	D	Qrt	Sxt	D	Qrt	Sxt
2D-PA-36	3.15	4.04	0.00	9.31	2.54	0.00
	(2.88)	(3.95)	(8.97)	(2.65)	(3.88)	(8.95)
1	4.329	1.011	0.000	6.571	0.839	0.000
	(2.157)	(3.969)	(8.931)	(1.775)	(3.851)	(8.927)
2	0.000	2.594	—	6.388	0.542	0.000
	(2.392)	(3.977)	—	(1.799)	(3.898)	(8.928)
3	7.267	2.060	0.000	6.118	0.175	0.000
	(2.152)	(3.998)	(8.935)	(1.785)	(3.852)	(8.928)
4	5.299	1.634	0.000	3.061	0.000	0.437
	(1.810)	(4.405)	(9.006)	(1.836)	(3.901)	(8.986)
5	0.000	1.015	—	0.000	4.106	—
	(1.282)	(3.866)	—	(0.833)	(3.915)	—
6	2.646	3.242	0.000	0.000	1.938	—
	(2.739)	(4.278)	(8.951)	(2.326)	(3.858)	—
7	0.000	0.070	—	0.000	0.493	—
	(2.359)	(2.372)	—	(2.358)	(3.829)	—
8	5.210	1.599	0.000	2.947	0.000	4.004
	(2.420)	(4.089)	(8.968)	(1.954)	(3.866)	(8.939)
9	2.930	1.726	0.000	0.748	0.000	1.132
	2.12	(4.454)	(9.023)	(2.178)	(3.899)	(9.002)
9a	2.391	2.569	0.000	0.000	2.798	3.137
	(2.682)	(4.4439)	(9.010)	(2.355)	(3.876)	(3.877)
10	0.000	0.957	—	0.603	0.000	1.682
	(2.476)	(3.923)	—	(1.921)	(3.901)	(9.008)
10a	3.148	1.945	0.000	0.000	3.151	—
	(2.572)	(4.514)	(9.012)	(2.362)	(3.879)	—
11	0.835	1.139	0.000	0.552	0.000	1.888
	(2.442)	(4.362)	(9.017)	(2.091)	(3.894)	(8.989)
11a	2.595	1.761	0.000	0.000	3.504	10.664
	(1.856)	(4.477)	(8.999)	(2.359)	(3.876)	(8.947)
12	1.026	1.033	0.000	2.306	0.000	1.874
	(2.406)	(4.488)	(9.012)	(2.816)	(3.949)	(8.990)
12a	2.018	1.603	0.000	0.000	3.718	—
	(1.867)	(3.946)	(8.995)	(2.358)	(3.876)	—
13	2.041	0.877	0.000	0.520	0.000	1.765
	(2.185)	(4.068)	(9.028)	(1.891)	(3.893)	(9.001)
13a	2.633	1.795	0.000	0.000	3.452	10.615
	(1.982)	(3.903)	(9.012)	(2.358)	(3.880)	(8.951)
14	0.000	5.327	—	0.000	4.053	—
	(1.375)	(3.923)	—	(2.336)	(3.866)	—
15	0.000	3.371	—	4.651	0.001	0.000
	(2.555)	(3.902)	—	(1.872)	(3.874)	(3.875)
16	0.000	1.984	—	1.794	0.000	7.097
	2.889	3.898	—	1.528	3.860	8.924

Therefore, DFT produces reliable energies for the high spin states and less reliable ones for the triplets and the broken symmetry singlet states. This could affect the relative energies of the states with different total spin. Since the amount of the static correlation decreases with the multiplicity, DFT as a single reference method will energetically favours the high spin states. Systems with singlet ground state detected at DFT level will maintain the singlet ground state at multireference level too. However, the systems presenting high spin ground state at DFT level could actually have lower multiplicity ground state when multireference methods are used. Therefore, for the systems with quintet ground state found at DFT level the additional CAS single point calculations were run to ensure the correct relative energies for the states with different multiplicities. The relative energies of singlet, triplet and quintet states are listed in the Table 3.

As seen, CAS calculations confirm all quintet ground states with only one exception, the nanoflake **1** where CAS predicts singlet ground state followed by the triplet and then quintet state. The lowest relative energy of quintet state is detected for **3** where the quintet–singlet gap is close to 10 kcal mol^{-1}. As seen from the Tables 1 and 3, the relative energies of the states with different multiplicities differ, although for the almost all high spin ground states the results of DFT and CAS calculations qualitatively agree one another.

This discrepancy is a results of the strong multireference character of triplet and especially singlet states of the substituted nanoflakes.

When revising the Table 4, it can be easily seen that the multireference character of the states with different spin decreases with multiplicity. This is reflected in CI expansion coefficients. As seen the contribution for dominant configurations increase with the state multiplicity. Squared CI expansion coefficients for the dominant configuration is around 0.2 for singlets, while for quintet states this value is around 0.9. Therefore, quintet states are mostly single reference by nature,

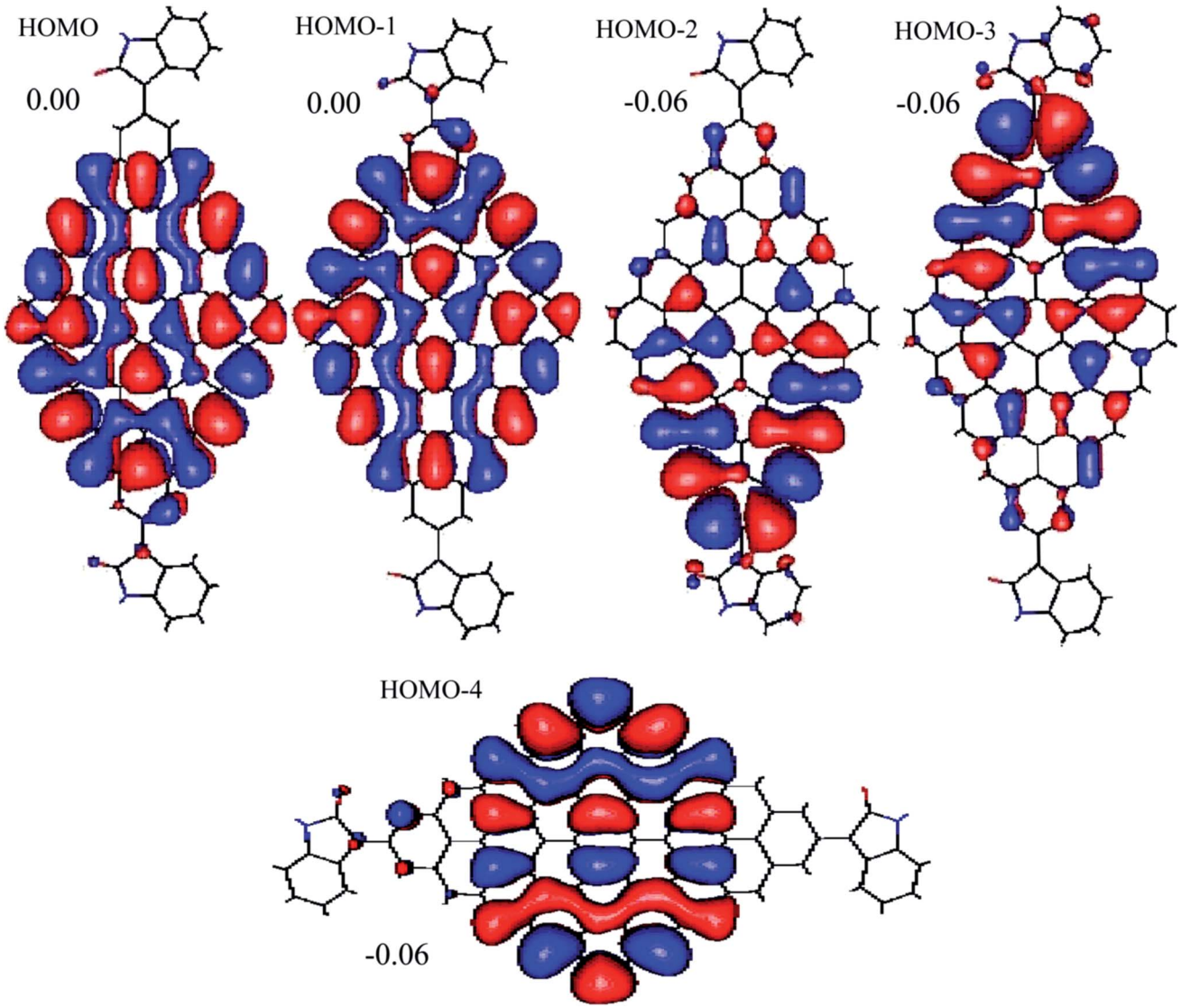

Fig. 4 Highest SOMO's of neutral state of **8** and their relative energies in eV.

while singlets are notably multiconfigurational. This conclusion is also confirmed by the close to theoretical $\langle S^2 \rangle$ expectation values for the high spin states.

Substituents not only change the multiplicity of the ground state of nanoflakes, they also notably change IP and EA of the nanoflakes (Table 5). As expected the electron donating group promote low IP and EA and the electron withdrawing substituents increases both IP and EA. Thus, the lowest IP (4.92 eV) was estimated for molecule **1** with donor 2-methylene-1,3-dithiole side groups, while the highest EA was found for nanoflake **5** (−4.49 eV) with pentacyanofulvene electron withdrawing substituents. These results are expected since 2-methylene-1,3-dithiole and pentacyanofulvane are the strongest donors and acceptors, respectively, out of all side groups selected for this study.

An interesting point is that the multiplicity of the ground state of the cations and anions is not determined by the multiplicity of the neutral molecule. The Table 6 shows the relative energies for the cationic and anionic states of different multiplicities for the studies nanoflakes. The structures were optimized starting from doublet and increasing multiplicity until energy start rising. As seen, in many cases the total spin of charged species does not obey a simple rule; spin of neutral state plus 1/2. Actually, the high spin ground state is more common for cations than for neutral species and for anions. In the case of molecule **8**, **11**, **12** and **13** the ground state is a singlet polyradicalic state, while the ground state of the cations are sextets with five unpaired electrons. The energy difference, between the high and the low spin states, however, does not exceed 2 kcal mol^{-1} (Table 2). Fig. 4 and 5 shows five highest SOMO's for the neutral ground state of **8** (singlet polyradicalic state) and the corresponding ground state of the cation (sextet state). As seen the electron detachment change notably the orbital topology. SOMO's of the neutral state are more disjoint than SOMO's of cationic state. Thus, in the neutral state only HOMO and HOMO−1 are similar in shape. On the other hand,

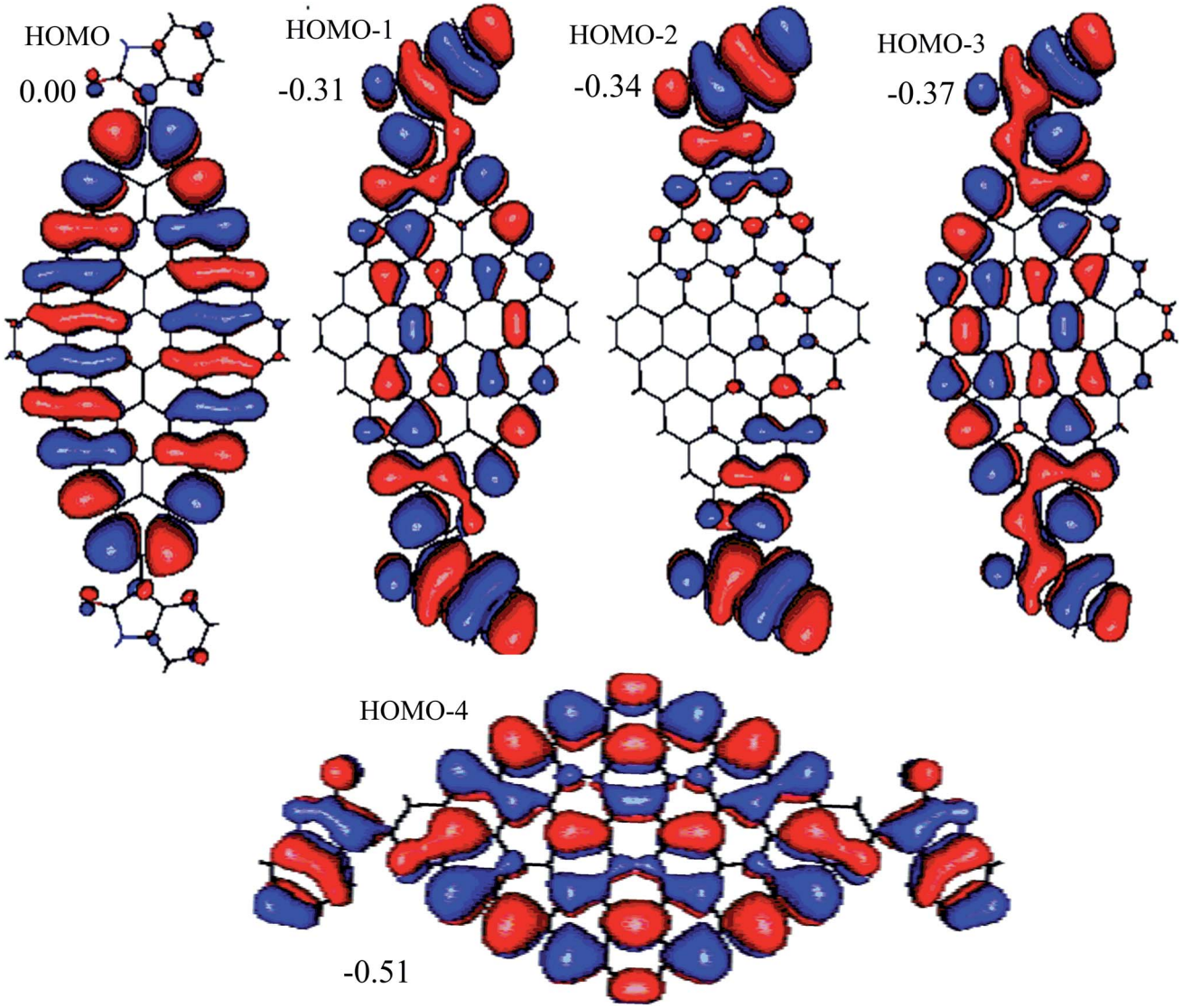

Fig. 5 Highest SOMO's of cationic state of **8** and their relative energies in eV.

in the cationic state only HOMO−2 differ significantly by topology from other SOMO's, thus explaining the high spin ground state for this molecule. Similar situation holds for other nanoflakes; **11**, **12** and **13** where the multiplicity of the neutral and the cationic states significantly differs.

Substituent affect both, the lowest excitation and the reorganization energies of substituted nanoflakes. The results are listed in the Table 7. As seen, in the vast majority of cases the substitution of pristine nanoflake increases the lowest excitation energies. The only exception is the nanoflake **14**, where the band gap slightly drops from 0.26 to 0.23 eV. The possible qualitative mechanism of this phenomenon can be understood from the Fig. 6 where two resonant structures of *p*-xylelene are shown, the aromatic and quinoid ones. *p*-Xylelene is the smallest and the simplest representative of **2D-PA** nanoflake series. As seen, the build-up of the unpaired electron density on methylene groups increases the aromaticity of the benzene ring opening up the HOMO–LUMO gap. Similar mechanism could be operational in the substituted nanoflakes. As seen from the Fig. 7 substituents delocalize a great deal of unpaired electron density increasing the HOMO–LUMO gap separation and, therefore, leading to the increase of the excitation energies. The exception of the nanoflake **14** can be explain by strong push–pull substituents of **14** which is known to reduce the excitation energies in organic molecules.[24]

Table 7 The lowest excitation (E_g) and reorganization energies λ_+ and λ_- (eV)

Structure	E_g (eV)	λ_+ (eV)	λ_- (eV)
2D-PA-36	0.26	0.0100	0.016
1	0.90	0.095	0.078
2	1.29	0.279	0.244
3	0.90	0.090	0.081
4	0.65	0.077	0.058
5	0.46	0.084	0.069
6	0.66	0.081	0.157
7	0.77	0.221	0.079
8	1.28	0.032	0.119
9	1.25	0.053	0.144
9a	1.16	0.035	0.058
10	1.26	0.072	0.105
10a	1.26	0.033	0.061
11	1.24	0.248	[a]
11a	0.28	0.030	0.041
12	1.24	0.055	0.056
12a	0.65	0.074	0.071
13	1.25	0.249	0.307
13a	1.26	0.030	0.042
14	0.23	0.182	0.055
15	1.29	0.319	0.217
16	1.28	0.255	0.272

[a] SCF not converged.

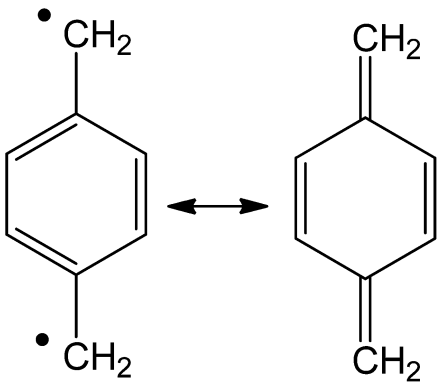

Fig. 6 Two resonance structures of *p*-xylelene.

Substitution also affects reorganization energies of the nanoflakes. As seen from the Table 7 any substituent increases the reorganization energy compare to the pristine nanoflakes, for both electron withdrawing and electron donating side groups. This phenomenon can be attributed to the less rigid structure of the substituted nanoflakes compared to the pristine one. However, different substituents increase the reorganization energy in different extent. The nanoflakes **9a**, **11a** and **13** show the smallest increase in reorganization energies compared to **2D-PA-36**, while in the case of **16**, **17**, **11**, **7** and **2** the reorganization energies increase by more than an order of magnitude for both hole and electron reorganization energies.

Fig. 8 and 9 show the correlation of the hole and the electron reorganization energies with −HOMO and −LUMO energies of the substituents, respectively. The −HOMO values approximates IP and −LUMO–EA of the substituent. As seen, although there is no clear correlation, one can appreciate the trend. In the case of the electron reorganization energies they tend to rise with −LUMO energies. The hole reorganization energy behave differently. They are elevated at low and high −HOMO energies passing through a minimum in between. Therefore, the electron reorganization energies tend to increase with an increase of electron withdrawing character of the substituent. Both strong electron donating and strong electron withdrawing groups rise the hole reorganization energy too. This behavior differs from that reported for cyano substituted anthracenes[25] where the cyanation reduces notably the reorganization energies of anthracene indicating that the same type of substituents can cause opposite effect on the reorganization energies in different systems.

Conclusions

The origin of the high spin ground state in **2D-PA-36** nanoflake and its derivatives is nondisjoint character of highest SOMO's orbitals, which explains the violation of the Ovchinnikov rule in this system. The results of DFT and CAS calculations qualitatively agree with each other in the prediction of the nature of the ground state. Substituents affect the nature of the ground state in different way. The electron withdrawing side groups, especially these with cyano substituents favor singlet ground state. The effect of electron donating groups is more erratic. They can promote both high and low spin ground state. Substituents change the topology of SOMO's thus modifying the exchange coupling between electrons. Depending on the substituent type, one or another spin state is favored. Substitution increase the

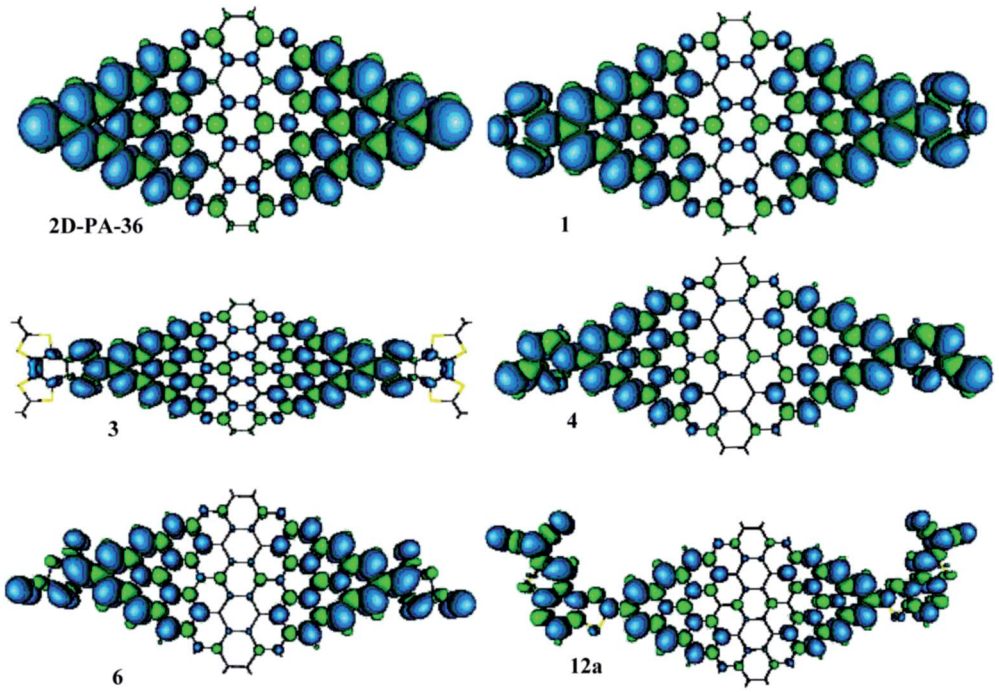

Fig. 7 Unpaired spin density in quintet ground states of pristine and substituted nanoflakes.

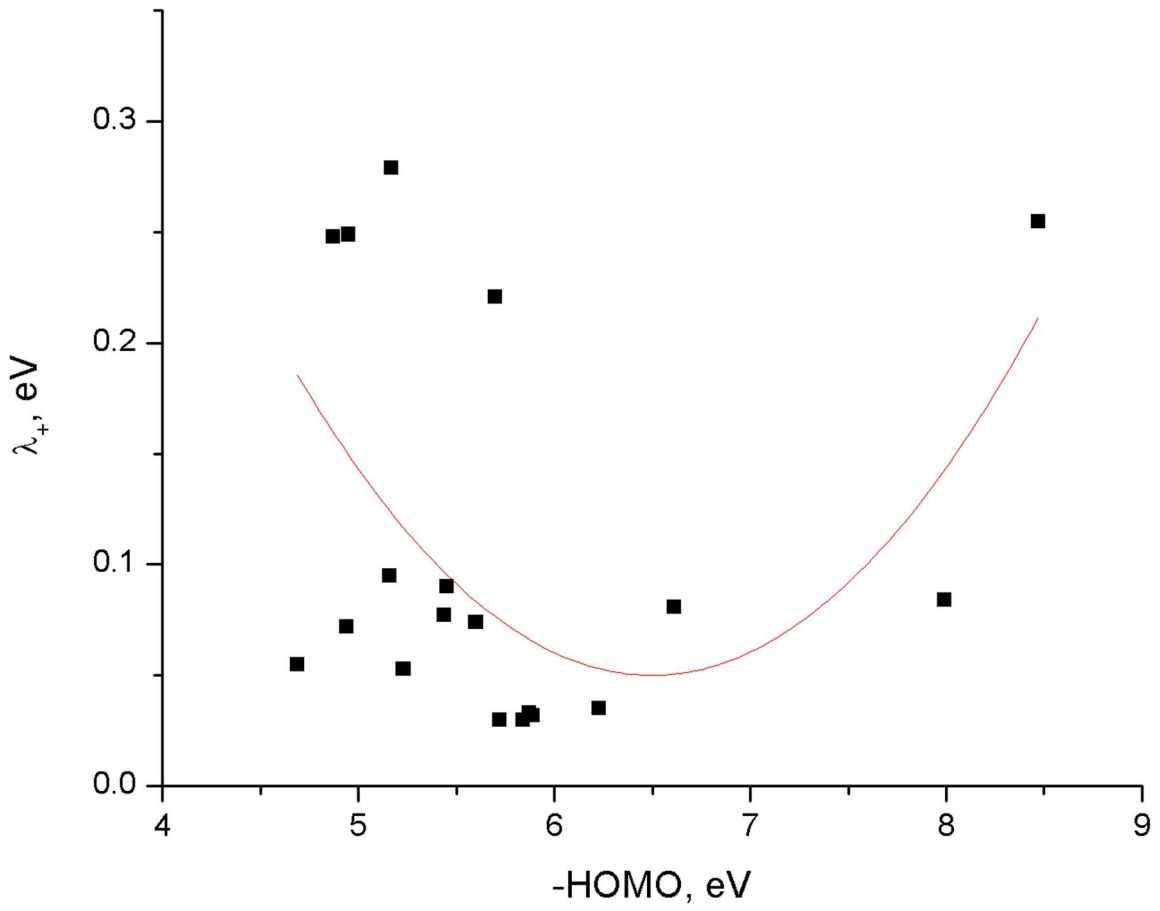

Fig. 8 The correlation between −HOMO and hole reorganization energies (eV).

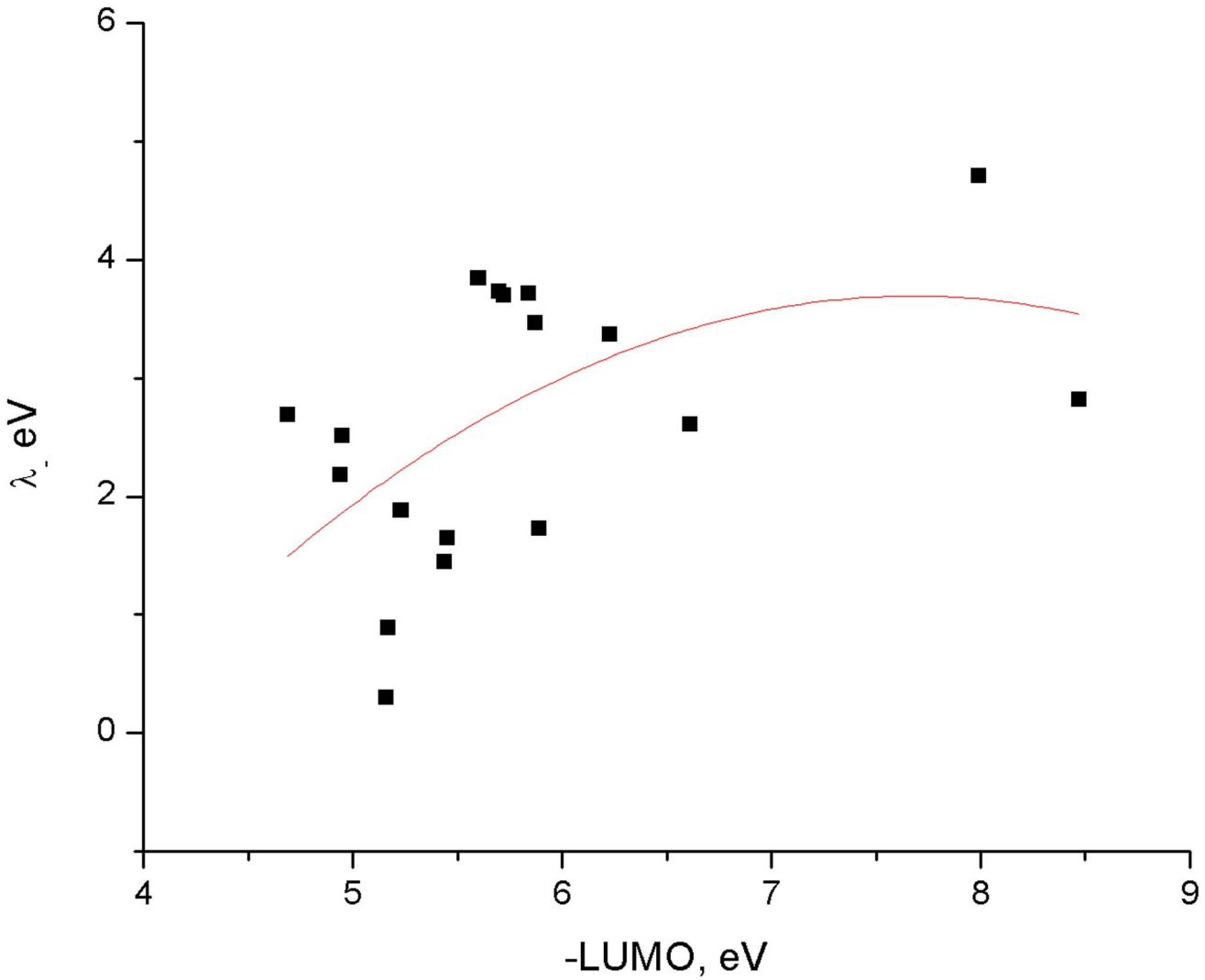

Fig. 9 The correlation between −HOMO and hole reorganization energies (eV).

band gaps in the nanoflakes by the delocalization of the unpaired electron density over the side groups. Substitution also affects reorganization energies of the nanoflakes. They increase the reorganization energy compare to the pristine nanoflakes, for both electron withdrawing and electron donating substituents. This phenomenon can be related to the less rigid structure of the nanoflakes bearing side groups compared to the pristine one. The rise of the reorganization energy also depends on the substituent nature.

Acknowledgements

We acknowledge the financial support from Program to Support Research and Technological Innovation Projects (PAPIIT) (grant IN100215/27) and we also would like to thank the General Direction of Computing and Information Technologies and Communication of the National Autonomous University of Mexico (DGTIC-UNAM) for the support to use the supercomputer facilities. A. E. Torres gratefully acknowledges Consejo Nacional de Ciencia y Tecnología (CONACyT) for a graduate scholarship (245467) and R. Flores states his gratefulness to CONACyT for the postdoctoral fellowship (173315).

References

1 U. Mehmood, A. Al-Ahmed and A. Hussein, *Renewable Sustainable Energy Rev.*, 2016, **57**, 550–561.
2 T. A. Skotheim and J. Reynolds, *Conjugated Polymers: Theory, Synthesis, Properties, and Characterization*, CRC Press, 2006.
3 A. K. Geim and K. S. Novoselov, *Nat. Mater.*, 2007, **6**, 183–191.
4 A. E. Torres, P. Guadarrama and S. Fomine, *J. Mol. Model.*, 2014, **20**, 1–9.
5 A. E. Torres and S. Fomine, *Phys. Chem. Chem. Phys.*, 2015, **17**, 10608–10614.
6 F. Plasser, H. Pasalic, M. H. Gerzabek, F. Libisch, R. Reiter, J. Burgdörfer, T. Müller, R. Shepard and H. Lischka, *Angew. Chem., Int. Ed.*, 2013, **52**, 2581–2584.
7 A. A. Ovchinnikov, *Theor. Chim. Acta*, 1978, **47**, 297.
8 W. T. Borden, H. Iwamura and J. A. Berson, *Acc. Chem. Res.*, 1994, **27**, 109.

9 A. E. Torres, R. Flores and S. Fomine, *Synthetic Met.*, 2016, **213**, 78–87.
10 R. Gutzler and D. F. Perepichka, *J. Am. Chem. Soc.*, 2013, **135**, 16585–16594.
11 D. A. Dougherty, *Acc. Chem. Res.*, 1991, **24**, 88–94.
12 W. T. Borden and E. R. Davidson, *J. Am. Chem. Soc.*, 1977, **99**, 4587–4594.
13 A. Rajca, *Chem. Rev.*, 1994, **94**, 871–893.
14 D. A. Dougherty, *Acc. Chem. Res.*, 1991, **24**, 88–94.
15 H. Meier, U. Stalmach and H. Kolshorn, *Acta Polym.*, 1997, **48**, 379–384.
16 J. M. Szarko, B. S. Rolczynski, S. J. Lou, T. Xu, J. Strzalka, T. J. Marks, L. Yu and L. X. Chen, *Adv. Funct. Mater.*, 2014, **24**, 10–26.
17 T. H. Dunning, *J. Chem. Phys.*, 1989, **90**, 1007–10238.
18 S. Grimme, J. Antony, S. Ehrlich and H. Krieg, *J. Chem. Phys.*, 2010, **132**, 154104.
19 M. J. Frisch, *et al.*, *Gaussian 09, Revision D.01*, Gaussian, Inc., Wallingford, CT, USA, 2009.
20 Y. Zhao and D. G. Truhlar, *Theor. Chem. Acc.*, 2008, **120**, 215–241.
21 D. S. Huh and S. J. Choe, *J. Porphyrins Phthalocyanines*, 2010, **14**, 592–604.
22 E. A. B. Kantchev, T. B. Norsten and M. B. Sullivan, *Org. Biomol. Chem.*, 2012, **10**, 6682–6692.
23 C. Wang, J. Zhang, G. Long, N. Aratani, H. Yamada, Y. Zhao and Q. Zhang, *Angew. Chem., Int. Ed.*, 2015, **54**, 6292.
24 J. Roncali, *Chem. Rev.*, 1997, **97**, 173–205.
25 Y. H. Park, Y.-H. Kim, S. K. Kwon, I. S. Koo and K. Yang, *Korean Chem. Soc.*, 2010, **31**, 1649–1656.